Hindawi
Advances in Materials Science and Engineering
Volume 2020, Article ID 5640561, 12 pages
https://doi.org/10.1155/2020/5640561

Research Article

Numerical Modeling of Seismic Responses and Seismic Measures of Tunnel Crossing a Fault Zone: A Case Study

Lin Li,[1] Liping Xian,[1] Chaofan Yao ,[2] Deping Guo,[3] and Chengliang Liu[1]

[1]*College of Civil Engineering, Sichuan Agricultural University, Ya'an 611830, China*
[2]*Key Laboratory of Transportation Tunnel Engineering, Southwest Jiaotong University, Ministry of Education, Chengdu 610031, China*
[3]*Sichuan Railway Investment Group Co., Ltd, Chengdu 610094, China*

Correspondence should be addressed to Chaofan Yao; yaochaofan@hotmail.com

Received 13 May 2019; Revised 1 February 2020; Accepted 3 February 2020; Published 8 April 2020

Academic Editor: Abílio De Jesus

The investigation shows that Longxi Tunnel, across a fault zone, was severely damaged during the 2008 Wenchuan earthquake, China. In this paper, the dynamic time history analysis method is used to study the seismic response characteristics of Longxi Tunnel and the aseismic effect of seismic measures. The interfaces of the fault are simulated by bonded interfaces. The results show that high earthquake intensity, high in situ stress, and fault zone are the main reasons for damage of Longxi Tunnel. The inconsistent motion response between the normal surrounding rocks and surrounding rocks within the fault zone resulted in the damage of Longxi Tunnel, and the maximum displacement difference reaches 50 cm. With the seismic measure by setting shake absorb layer and seismic joints, the tunnel has better performance: the maximum peak internal force of the tunnel structure is reduced by about 26% and the acceleration is reduced by 30%. Seismic measures should not only be considered within fault zones but also extend to adjacent surrounding rocks. In this study, the fault seismic measures of Longxi Tunnel should be no less than 4.0 times the tunnel diameter.

1. Introduction

Tunnels are deemed to perform much better than surface structures during earthquakes [1–5], and their seismic capacities improve with the increase of embedment depths [6, 7]. However, the observations after earthquakes with an acceleration larger than 0.2 g found that severe damage occurred in tunnels due to strong earthquake shaking [8, 9]. Severe damage usually occurs due to poor geological conditions, such as fault, portals, unsymmetrical loading section, and shallow buried depth [10–14].

A lot of scholars have contributed to tunnel seismic damage mechanisms and seismic measures. The authors of [15–17] summarized 94 tunnels damaged by earthquake. It was found that those with overburden soil less than 50 m accounted for 35% of the total tunnels. After the 1995 Kobe earthquake in Japan, Yashiro et al. [9] found that the mountain tunnels in the epicentral area were damaged severely owing to high intensity and existence of faults. Wang et al. [18] made assessment of damage of mountain tunnels after 1999 Chi-Chi earthquake, Taiwan. The results showed that 26% of the 50 tunnels located within 25 km of the fault were severely damaged and 22% of them were moderately damaged. Knotoe et al. [19] and O'Rourke et al. [20] conducted case studies of the twin tunnels in Bolu highway. It showed that the tunnels experienced a wide range of damage during the 1999 Duzce earthquake in Turkey.

During the 2008 Wenchuan earthquake in China, a lot of tunnels were damaged severely. Longxi Tunnel in Dujiangyan-Wenchuan highway was a representative seismic damaged tunnel (Figure 1). The tunnel mainly experiences three types of damage: (1) longitudinal lining crack, (2) inclined lining crack, and (3) local lining failure. The lining cracks are about 2-3 mm wide, distributing around the fault. The local failure mainly occurred at the tunnel vaults

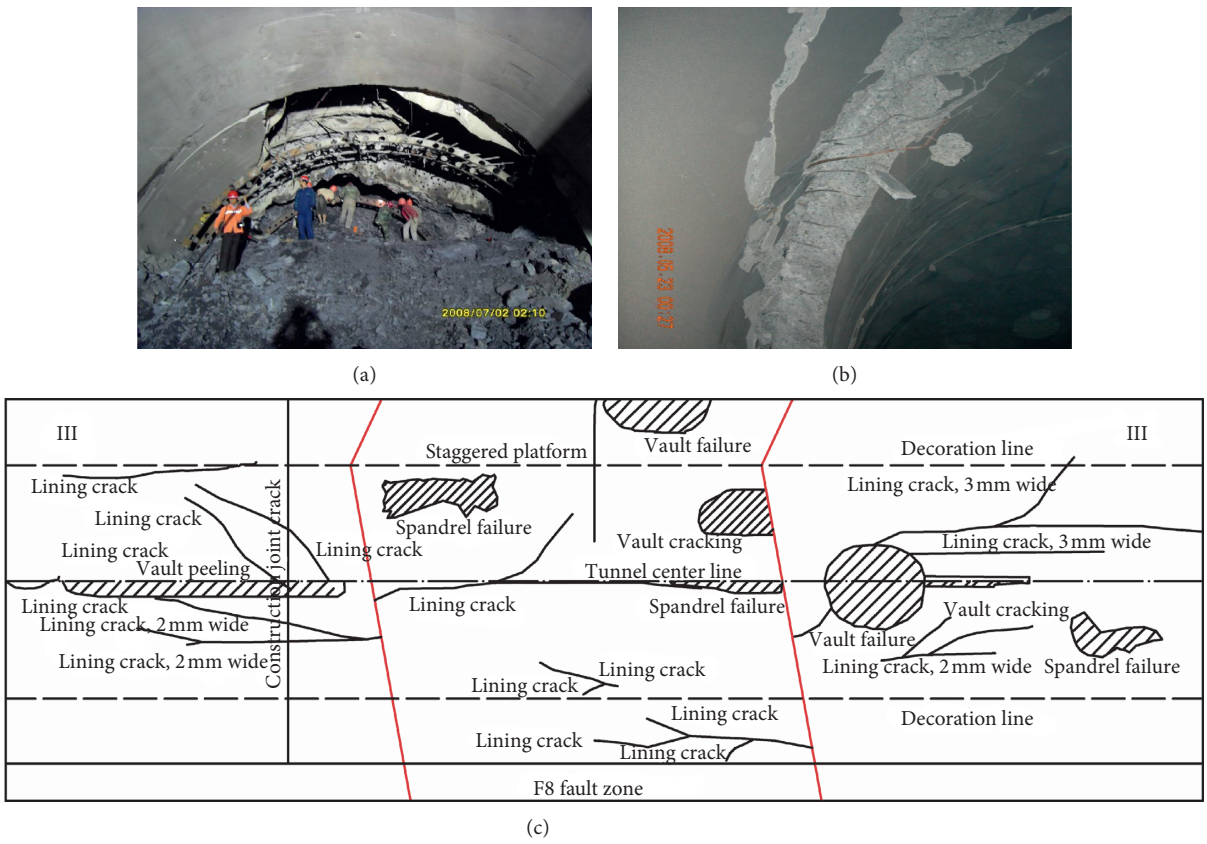

Figure 1: Seismic damage of Longxi Tunnel. (a) Lining collapse. (b) Lining dislocation. (c) Damage near the fault zone.

and spandrels (Figure 1(a)). Besides, lining dislocation was also observed due to the large shear force caused by faulting (Figure 1(b)). Li [21, 22] analyzed the deformation and damage characteristics of Longxi Tunnel and performed parametric studies, such as seismic intensity, seismic wave propagation direction, fault zone, and surrounding rock quality. Wang et al. [23] investigated and preliminarily analyzed the seismic damage of highway tunnels in Wenchuan earthquake-stricken areas, including Longxi Tunnel. Damage was classified as four types: no damage, minor damage, moderate damage and severe damage. Lai et al. [24] conducted a seismic investigation on 52 tunnels after the 2008 Wenchuan earthquake. It was found that the most serious tunnel damage was the fault fracture zone, for example, Longxi Tunnel. Yu et al. and Kusakabe et al. [25, 26] found that cracks in different sections of the cavern occurred through the investigation of the damage of the Shaohuopin tunnel and the linings near the fault zone collapsed. Yu et al. [25] assessed the seismic damage observed in Longxi Tunnel and evaluated the influence of the longitudinal and vertical motions on the seismic response. For aseismic measures, previous studies [27, 28] have been conducted to investigate the dynamic behavior of tunnel with seismic measures. Chen and Shen [29] studied the isolation layer which was one of the countermeasures to enhance seismic safety of tunnels. Li and He [30] pointed out that different seismic measures were suitable for different tunnel working conditions based on the shaking table test and damage investigations after the 2008 Wenchuan earthquake.

Many researchers have contributed to the seismic damage characteristics of tunnels due to earthquake, especially Longxi Tunnel after the 2008 Wenchuan Earthquake, China. However, effective seismic measures have not been proposed and their effects on tunnel response are still not clear. In this study, numerical modeling was conducted to investigate the seismic response of Longxi Tunnel during the 2008 Wenchuan earthquake. A bonded interface was adopted to model the interfaces of fault. Two seismic measures are examined, including shake absorb layers and seismic joints. The major objectives of this study were (1) to investigate the influence areas of seismic responses of tunnel due to fault and (2) to explore the effects of seismic measures on seismic response of Longxi Tunnel.

2. Engineering Situation

2.1. Engineering Geology. Longxi Tunnel in Dujiangyan-Wenchuan Highway is 5 km far away from the epicenter of the Wenchuan earthquake, located between Longxi town and Yingxiu town (Figure 2(a)). The basic earthquake intensity degree is classified as VII. The tunnel site is located between Yingxiu Fault F3 and Longxi Fault F2. The tunnel crosses F8 Fault and some secondary small faults, as shown in Figure 2(b). The surrounding rocks are mainly soft rocks, which are classified as Grade IV;. The gas concentration in the tunnel is up to 18%, which is called the "Powder Keg in Western Sichuan Province." Therefore, it is a highway tunnel

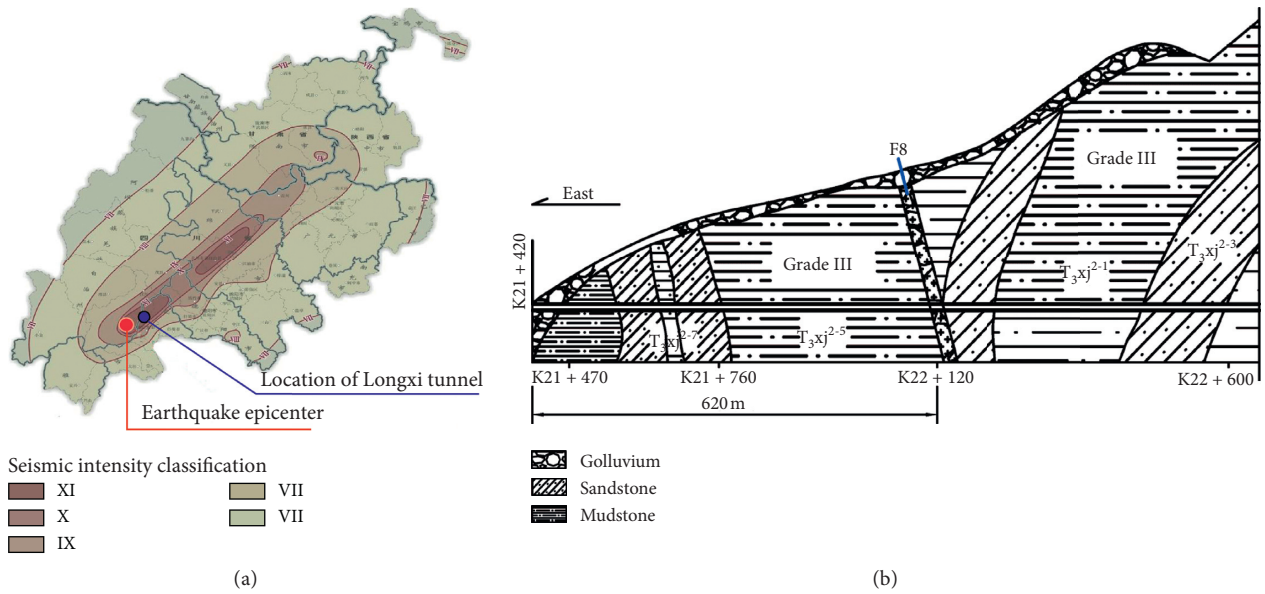

Figure 2: (a) Location and (b) profile diagram of Longxi Tunnel.

integrating high gas concentration, large ground stress, and big geological faults.

2.2. Distribution of Tectonic Stress Fields. The tunnel construction site is located at the big fault zone of Longmen Mountains, with a complex geological structure. It is in the area where the faults are densely distributed. The fault zone has a relatively high stress field. According to a research report on ground stress measurement of Longxi Tunnel (Figure 3 and Table 1), the maximum principal stress is up to 26.4 MPa in the left tunnel and that is about 25 MPa in the right tunnel. The adjacent Futang tunnel and Headrace tunnel have experienced rock burst during construction, which indicates that the tunnel was constructed in a less favorable stress field environment [30].

3. Numerical Modeling

3.1. Dynamic Numerical Model and Parameters. The numerical model and its boundary conditions are displayed in Figure 4. In this study, the finite element (FE) code ANSYS is applied to build the three-dimensional model and to mesh the unit. Besides, the finite difference (FD) code FLAC^{3D} is used to calculate the numerical model. A hexahedral element was adopted to model the surrounding soil, using the Mohr–Coulomb constitutive model, while the tunnel lining was modelled as elastic elements. A bonded interface was used to model the interfaces of fault. The solving was based on the dynamic module in FLAC^{3D}. The viscous boundary conditions were used, which considered the infinite field, as shown in Figure 4(b). The details of the boundary conditions will be illustrated later.

In the dynamic numerical model of Longxi Tunnel, it is considered that the F8 fault zone has a dip angle of 72° and a width of 8 m. The area is dominated by granite strata in the Jinning Period. The fault zone is filled with gravelly soils of granites. According to previous geological investigation, the fault is under the low strain rate [31]. Therefore, there is no significant difference between dynamic mechanical parameters and static mechanical parameters of the rock. Static parameters of the rock are used in the numerical simulation, and the specific calculation parameters are listed in Table 2.

3.2. Dynamic Damping. In the dynamic analysis, the Rayleigh damping is commonly used in engineering. During the setting of Rayleigh damping, the intermediate frequency must be selected initially. As for geological bodies, damping is generally unaffected by the frequency and the intermediate value of frequency range in numerical simulation is often selected as the intermediate frequency value. In the dynamic equation, damping matrix C is related to stiffness matrix K and mass matrix M. They should be referred to as the following [33]:

$$C = \alpha M + \beta K, \tag{1}$$

where α and β are the mass ratio damping coefficient and the stiffness ratio damping coefficient, respectively.

4. Fault Zone Simulation

In this paper, the combination of solid elements and contact surface elements were used to simulate the fault fracture zone. The contact surface element was composed of a series of three-node and three-untied elements. The triangular area was distributed to each node by the contact surface element. Each contact surface node had a relevant denoted area. The contact surface with a Coulomb sliding contact element mainly had two states, including mutual contact state and relative sliding state. Its constitutive model is presented in Figure 5(a).

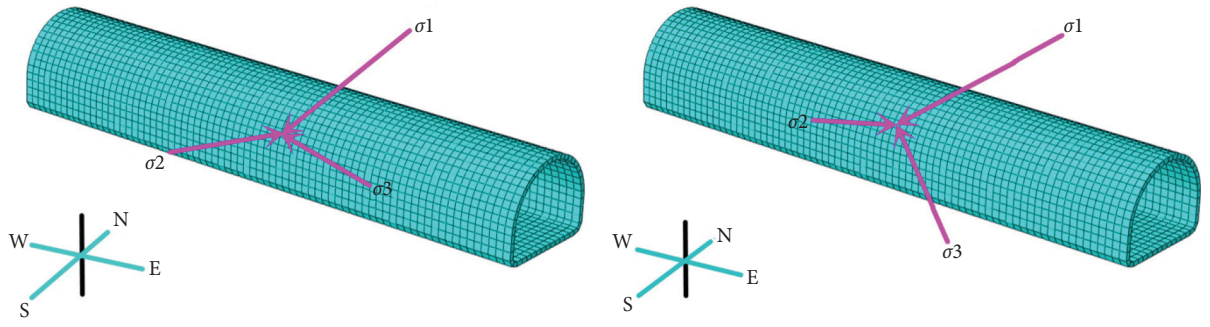

Figure 3: Relationship between main direction of ground stress and tunnel axis. (a) Left tunnel. (b) Right tunnel.

Table 1: Test results of ground stress in Longxi Tunnel (updated from Xu et al. [31]).

Location of test point	Stress item	Maximum principal stress	Intermediate principal stress	Minimum principal stress
Left tunnel	Measurement value (MPa)	26.4	13.6	12.1
LK23 + 810~815	Direction (°)	N36.8 E	N66.1 E	N48.8 W
	Dip angle (°)	21.8	−65.4	−10.9
Right tunnel	Measurement value (MPa)	25.1	16.8	9.4
	Direction (°)	N49.6 E	N63.8 W	N18.9 E
RK22 + 345	Dip angle (°)	58.7	13.6	−27.6

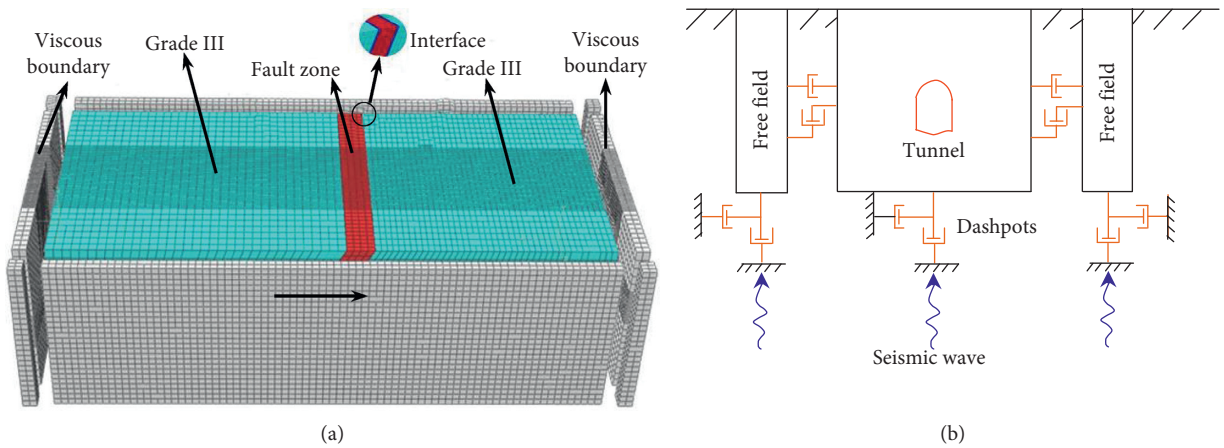

Figure 4: (a) Dynamic numerical model and its (b) boundary conditions.

Table 2: Properties of rock material (updated from Yu [32]).

Rock type	Density (g·cm^3)	Elastic modulus (GPa)	Poisson ratio	Cohesion (kPa)	Internal friction angle (°)
Grade III	2.20	8	0.30	550	40
Fault zone	1.80	1	0.4	250	21

The normal and shear forces that describe the elastic interface response are determined at calculation time $(t + \Delta t)$ using equations (2) and (3):

$$F_n^{t+\Delta t} = K_n u_n A + \sigma_n A, \tag{2}$$

$$F_{si}^{t+\Delta t} = F_{si}^{t} + Ks\Delta u_{si}^{t+0.5\Delta t} A + \sigma_{si} A, \tag{3}$$

where $F_n^{t+\Delta t}$ is the normal force at time $(t + \Delta t)$, $F_{si}^{t+\Delta t}$ is the shear force vector at time $(t + \Delta t)$, u_n is the absolute normal penetration of the interface into the target face, Δu_{si} is the incremental relative shear displacement vector, σ_n is the additional normal stress added due to interface stress initialization, K_n is the normal stiffness, K_s is the shear stiffness, σ_{si} is the additional shear stress vector due to interface stress

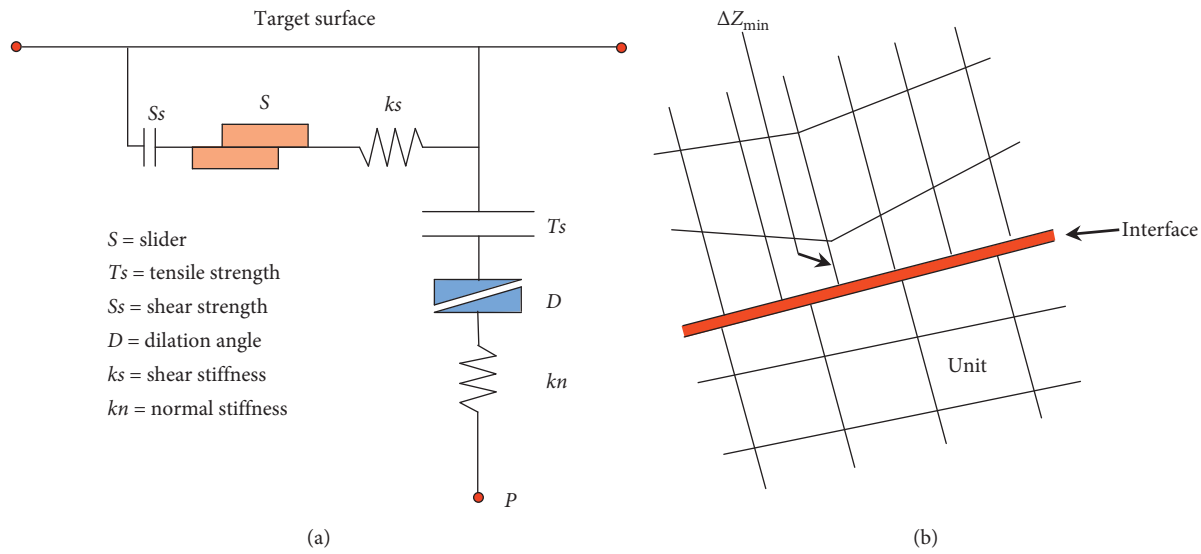

Figure 5: Details of the numerical model. (a) Constitutive model of interface between the fault zone and rock mass. (b) The minimum size in normal direction at the interface.

initialization, and A is the representative area associated with the interface node.

The normal stiffness and tangential stiffness of the contact surface are calculated as follows:

$$K_s = K_n = 10 \max\left[\frac{(K + (4/3)G)}{\Delta Z_{\min}}\right], \tag{4}$$

where K is the bulk modulus, G is the shear modulus, and $\Delta z_{\min}$ is the smallest dimension on the connecting area in the normal direction of the contact surface, as shown in Figure 5(b).

5. Dynamic Boundary Conditions and Failure Criteria

The dynamic boundary condition must be considered to absorb incident waves from the inside of the model. The viscous boundary is realized by arranging independent damping cylinders in the normal and tangential directions of the boundary to absorb incident waves from the inside of the model (Figure 4(b)). The viscous boundary is used in the dynamic calculation, i.e., the same attribute element as the grid in the domain is set outside the boundary to simulate the infinite domain. The element is connected with the infinite domain boundary element by elastic and viscous elements in order to absorb the reflected energy from the boundary. The force between the infinite domain element and the boundary element is calculated using equations (5)–(7):

$$F_x = -\rho Cp\left(v_x^m - v_x^{ff}\right)A + F_x^{ff}, \tag{5}$$

$$F_y = -\rho Cs\left(v_y^m - v_y^{ff}\right)A + F_y^{ff}, \tag{6}$$

$$F_z = -\rho Cs\left(v_z^m - v_z^{ff}\right)A + F_z^{ff}, \tag{7}$$

where ρ is the density, Cs and Cp are the medium transverse wave velocity and longitudinal wave velocity, respectively, v^m is the velocity in all directions of boundary nodes inside and outside the domain, v^{ff} is the velocity in all directions of corresponding nodes outside the domain, and F^{ff} is the corresponding node force of units outside the domain.

In the process of dynamic calculation, the classic Mohr–Coulomb strength criterion is adopted and the yield function [34] is calculated using equations (8) and (9):

$$f_s = \sigma_1 - \sigma_3 + 2c\sqrt{N_\varphi}, \tag{8}$$

$$f_t = \sigma_3 - \sigma_t, \tag{9}$$

where σ_1 and σ_3 are maximum and minimum principal stresses, respectively, φ is the friction angle, c is cohesive force, σ_t is the rock tensile strength, and N_φ is the coefficient and is denoted by

$$N_\varphi = \frac{1 + \sin\varphi}{1 - \sin\varphi}. \tag{10}$$

When the stress at a certain point in the rock mass is met, if $f_s < 0$, shear failure occurs and if $f_t > 0$, tensile failure occurs.

6. Earthquake Parameters

During the Wenchuan earthquake, Longxi Tunnel was located at the IX to X degree area. In this paper, Wolong seismic wave (east-west direction) monitored in Wolong Station is selected for calculation. In the calculation of the seismic peak acceleration, the actual seismic intensity is considered. With the peak acceleration of 600 gal and the time of 20 s, the corrected and filtered acceleration time history and Fourier transform are shown in Figure 6 [21].

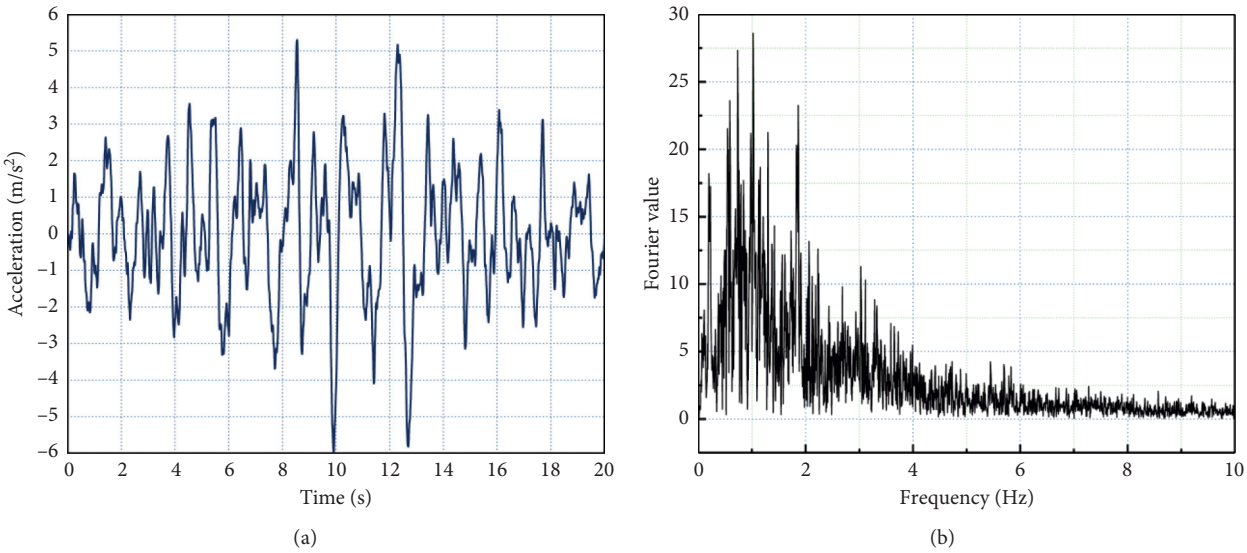

Figure 6: (a) Wenchuan seismic wave. (b) Fourier transform curve.

7. Results and Discussions

In the dynamic time history analysis, the objectives are to study the earthquake damage characteristics of Longxi Tunnel during the Wenchuan earthquake and the anti-shock effects of seismic measures, including shock absorption layer and seismic joints. The main seismic response information is measured in the monitoring points. When choosing the monitoring points, both the spatial distribution of dynamic responses and effects of the fault should be considered. Therefore, three types of monitoring points have been selected: (1) longitudinal monitoring points, (2) vertical monitoring points, and (3) special monitoring points around the fault. The longitudinal test points are numbered from S1 to S5 horizontally with an interval of 25 m, while the vertical ones are numbered from G1 to G8, as displayed in Figure 7(a). Besides, two pairs of special monitoring points C1 and C2 as well as C3 and C4 in the fault zone and the surrounding rock are set in order to test the relative relationship between the fault zone and the surrounding rock. Also, the seismic layer and seismic joint model are shown in Figure 7(b).

7.1. Acceleration Responses. The obtained response characteristics of the tunnel acceleration after the earthquake are displayed in Figure 8. Figures 8(a) and 8(b) show that the fault zone has similar spectral response characteristics with other surrounding rocks. However, because of the existence of high damping force, the regional fault zone has much larger frequencies. The acceleration response characteristic value of the tunnel surrounding rock in the fault zone is relatively high, with a maximum peak value of 1380 gal, which is 1.8 times compared with other surrounding rocks. The acceleration peak value of the tunnel is obviously reduced after seismic layers (see Figure 8(c)) and seismic joints are set (see Figure 8(d)), and the decrements are about 32% and 21%, respectively. The seismic layer has a relatively better effect on reducing the peak acceleration peak value.

The acceleration response characteristics of the tunnel roof along the tunnel axis are shown in Figure 9. It can be seen from Figure 9(a) that the fault zone and adjacent fault zones have a larger acceleration distribution within the range of about 4.0 times the tunnel diameter, showing normal distribution characteristics. The seismic layer has an obvious effect on the transition section of the fault zone (Figure 9(b)), while the impact of seismic joints is mainly within the range of 0.5 times the hole diameter of the seismic joint (Figure 9(c)). It is recommended to set the seismic joints at the distance of 0.5 times the tunnel diameter.

7.2. Seismic Displacement Characteristics. The displacement results of surrounding rocks after the Wenchuan earthquake are presented in Figure 10. The calculation results show that the displacements of the tunnel are relatively high. The displacement response trend of the tunnel and its surrounding rocks are basically the same, indicating that the tunnel structure displaces along with the surrounding rock. The result agrees with those found by He and Koizumi [35]. However, because of the poor quality of the surrounding rock in the fault zone, the seismic response of the fault zone is asynchronous with sections with normal surrounding rocks during earthquake. Figure 11 presents the displacement response of the tunnel roof with and without seismic measures. It can be seen from Figure 11(a) that the displacement response of the fault zone is apparent, the maximum displacement value reaches 1.2 m, and the displacement value of sections with normal surrounding rocks is relatively small. However, the displacement value of the surrounding rock in the fault zone is obviously lagging behind, and the relative displacement generated by such hysteresis is 0.8 m. After the installation of shake absorb layers and seismic joints, the relative displacement value

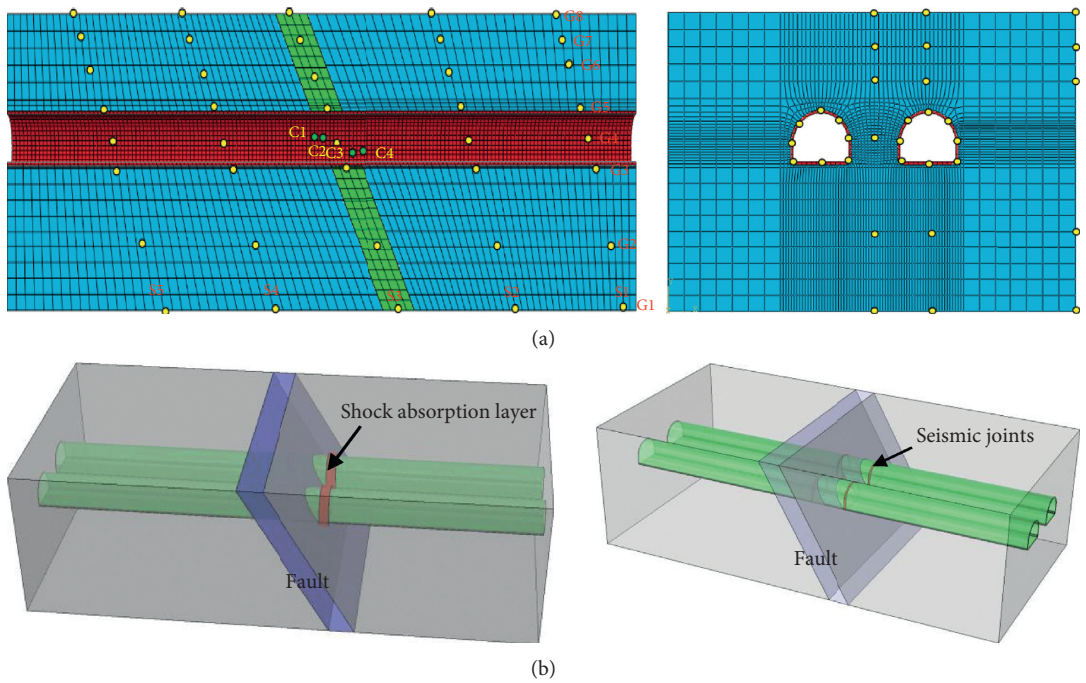

Figure 7: Monitoring points and setting of seismic measures in the numerical model. (a) Monitoring points. (b) Seismic measures.

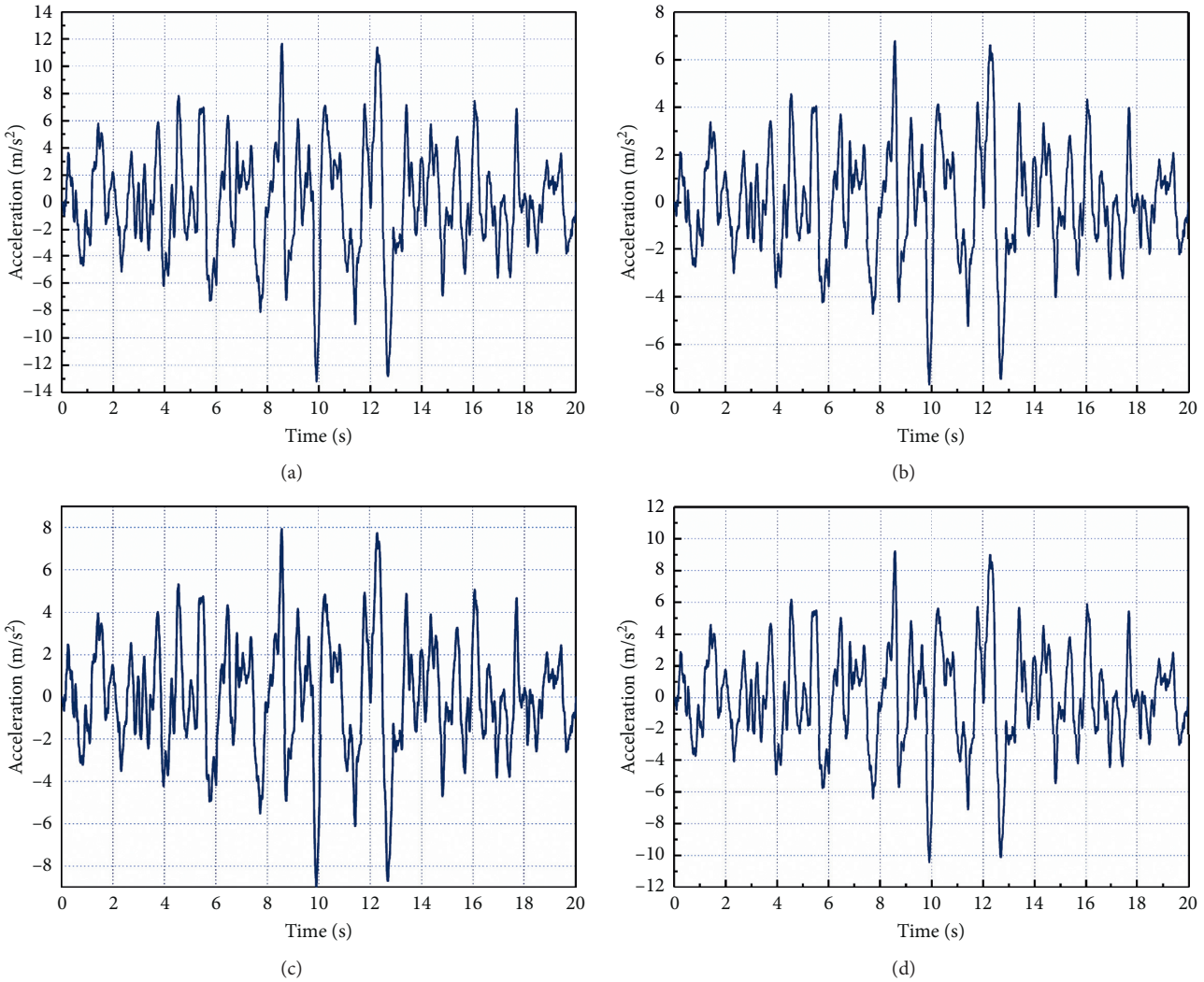

Figure 8: Acceleration responses. (a) Fault zone. (b) Rock mass. (c) Fault zone with hock absorption layer. (d) Fault zone with seismic joints.

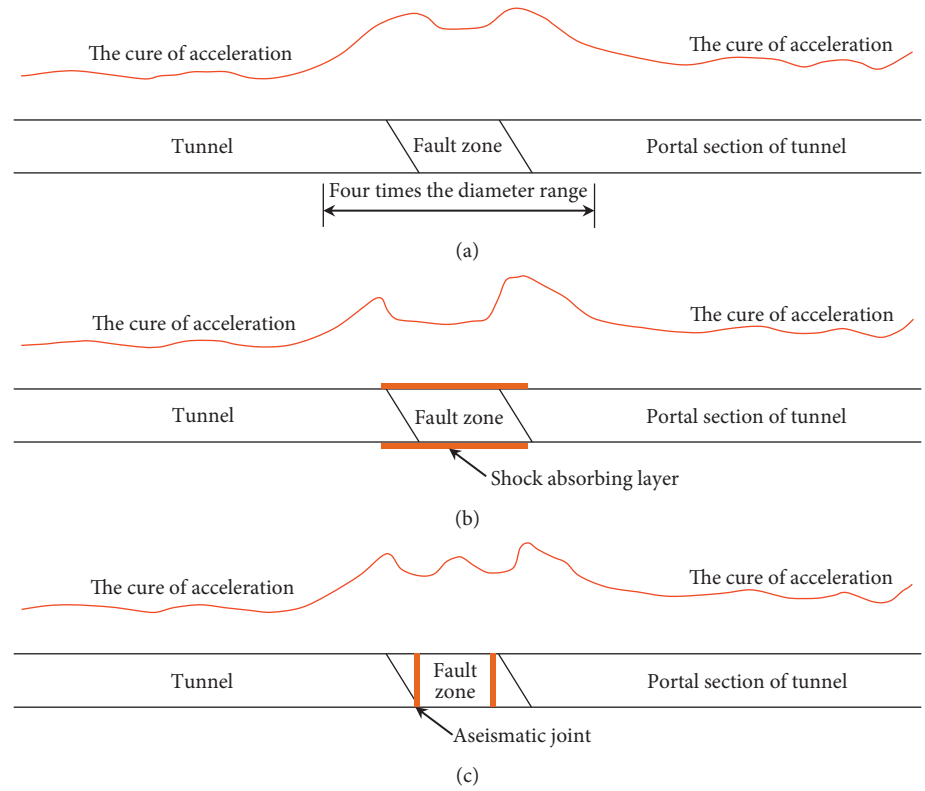

Figure 9: Peak acceleration distribution at the tunnel roof (left tunnel). (a) Without seismic measurements. (b) With shock absorption layer. (c) With aseismic seam.

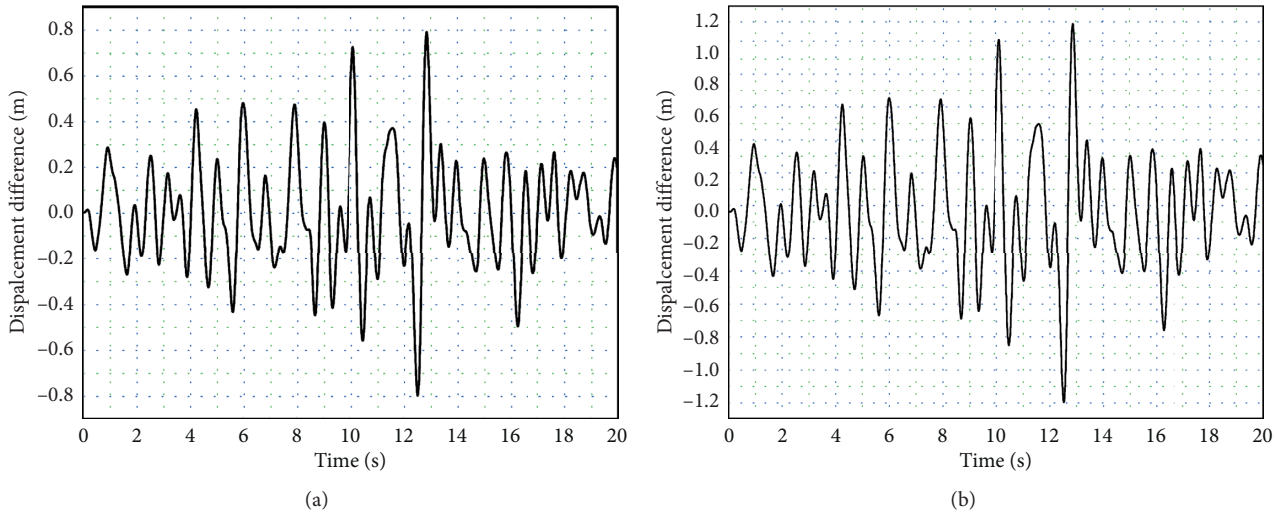

Figure 10: Displacement responses of surrounding rocks. (a) Normal surrounding rock. (b) Surrounding rock within the fault zone.

basically remains the same (Figures 11(b) and 11(c)), which indicates that such two seismic measures cannot reduce the relative displacement between sections with normal surrounding rocks and fault zones, and the main reason of relative displacement is the quality difference of surrounding rocks, so in the fault zone, grouting and other measures shall be taken together to reinforce surrounding rocks.

7.3. Bending Moment Distribution of Tunnel. The calculated bending moment of the left and right tunnels at 9.8 s and 12.7 s is shown in Figure 12. The positive value of bending moment is defined when the outer surface is in tension. It can be seen from Figure 12 that the tension and compression cyclic loading exists in the tunnel structure. The dynamic loading in the tunnel roof and the tunnel waist is small, and

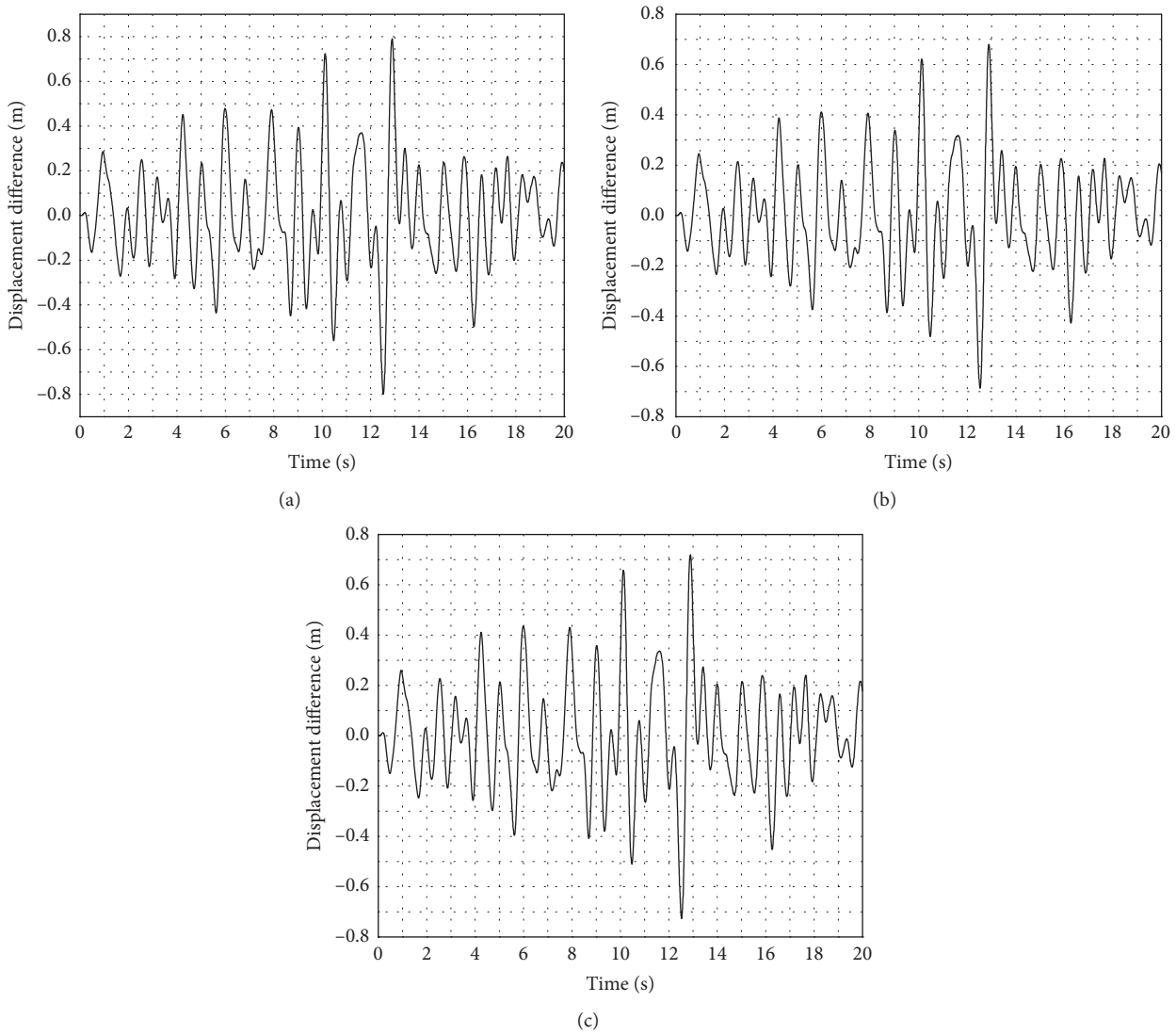

Figure 11: Displacement responses of the tunnel roof. (a) Without seismic measures. (b) With shock absorption layers. (c) With seismic joints.

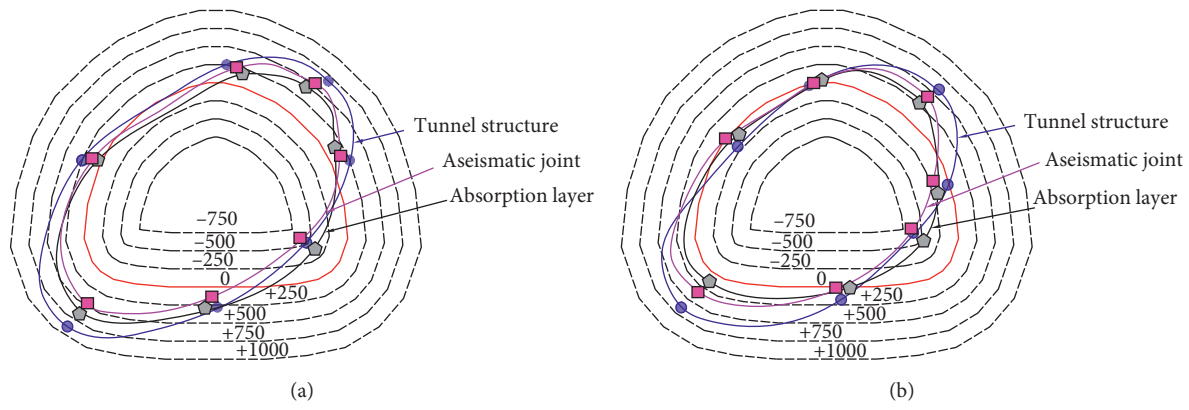

Figure 12: Continued.

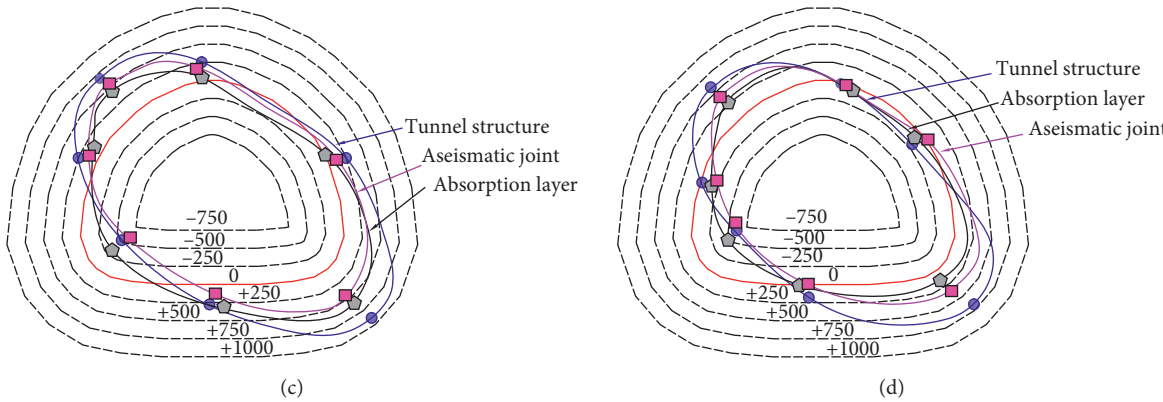

Figure 12: Bending moment distributions at 9.8 s and 12.7 s. (a) Left tunnel at 9.8 s. (b) Right tunnel at 9.8 s. (c) Left tunnel at 12.7 s. (d) Right tunnel at 12.7 s.

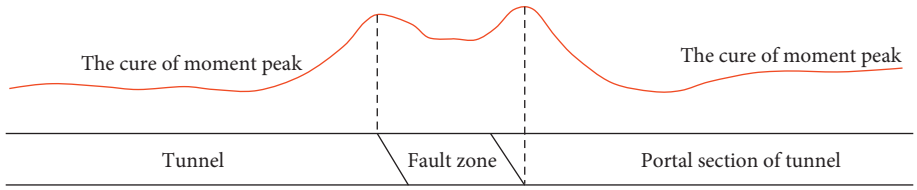

Figure 13: The peak bending moment distribution at the top left corner of the left tunnel at 12.7 s.

the dynamic loading value in the (left and right) tunnel foot and tunnel shoulder is relatively large. After installing the shake absorb layers and seismic joints, the internal force distribution trends are not changed. However, the peak value will be obviously reduced and values in the lower right corner are reduced by about 28% and 42%, respectively.

Figure 13 displays the peak bending moment distribution at the top left corner of the left tunnel at 12.7 s. It shows that the peak bending moment is gently distributed at sections with normal surrounding rocks. However, the peak bending moment significantly increases when the tunnel crosses the fault zone. According to the incident direction of Wenchuan Wolong seismic wave (east-west direction), the seismic load distribution in the left hole is larger than that in the right hole. The maximum bending moment in the left tunnel reaches 978.4 KN m in the fault zone, which occurred at the lower right corner of the tunnel. The results indicate that the bending moment responses depend on the quality of the surrounding rocks. The better the surrounding rock quality is, the lower the bending moment, and vice versa.

8. Conclusions

In this study, numerical modeling is performed to investigate the seismic responses of Longxi Tunnel crossing a fault zone during the 2008 Wenchuan earthquake. A bonded interface was adopted to model the interfaces of fault. Besides, the effects of two seismic measures on tunnel responses are examined, including shake absorb layers and seismic joints.

The fault has great influence on the seismic responses of the tunnel. The inconsistent surrounding rock in the vicinity of the fault leads to a displacement difference up to 50 cm, which can cause severe damage to the tunnel. It agrees with the field observations after the earthquake. With the seismic measures, the tunnel performs much better. The functions of the seismic measures are to reduce the internal forces and accelerations rather than decreasing the dynamic displacements. The case study shows that more than one-quarter of the maximum internal force and acceleration can be reduced by the seismic measures. Besides, the seismic measures should not only be considered within fault zones but should also extend to adjacent surrounding rocks. The case study indicates that the extended length should be no less than 4.0 times the tunnel diameter.

Data Availability

The data used to support the findings of this study are included within the article.

Conflicts of Interest

The authors declare that there are no conflicts of interest regarding the publication of this paper.

Acknowledgments

This study was financially supported by the National Natural Science Foundation of China under Grant no. 51708373 and the China Postdoctoral Science Foundation under Grant no. 2019M663901XB. The authors thank the National Natural Science Foundation of China and all who have contributed to this study.

References

[1] A. Toshihiro and S. Yutaka, "Damage to mountain tunnels in hazard area," *Soils and Foundations*, vol. 36, pp. 301–310, 1996.

[2] Y. Luo, J. Chen, P. Huang, M. Tang, X. Qiao, and Q. Liu, "Deformation and mechanical model of temporary support sidewall in tunnel cutting partial section," *Tunnelling and Underground Space Technology*, vol. 61, pp. 40–49, 2017.

[3] J. Takemura, C. Yao, and O. Kusakabe, "Development of a fault simulator for soils under large vertical stress in a centrifuge," *International Journal of Physical Modelling in Geotechnics*, pp. 1–36, 2019.

[4] C. Yao and J. Takemura, "Using laser displacement transducer scanning technique in centrifuge modeling of reverse fault–foundation interaction," *Soil Dynamics and Earthquake Engineering*, vol. 121, pp. 219–232, 2019.

[5] C. Yao and J. Takemura, "Centrifuge modeling of single piles in sand subjected to dip-slip faulting," *Journal of Geotechnical and Geoenvironmental Engineering*, vol. 146, no. 3, Article ID 04020001, 2020.

[6] J. X. Lai, S. Y. He, J. L. Qiu et al., "Characteristics of seismic disasters and aseismic measures of tunnels in Wenchuan earthquake," *Environmental Earth Sciences*, vol. 76, no. 2, pp. 1–19, 2017.

[7] A. Vieria, J. V. Lemos, L. R. Sousa et al., "Numerical and analytical modelling of shallow tunnels under seismic loading," in *Proceedings of the XVICSMGE TC4 Satellite Conference Lessons Learned from Recent Strong Earthquakes*, pp. 203–208, Istanbul, Turkey, 2001.

[8] M. Genis, "Assessment of the dynamic stability of the portals of the Dorukhan tunnel using numerical analysis," *International Journal of Rock Mechanics & Mining Sciences*, vol. 47, no. 8, pp. 1231–1241, 2010.

[9] K. Yashiro, Y. Kojima, and M. Shimizu, "Historical earthquake damage to tunnel in Japan and case studies of railway tunnels in the 2004 Niigataken-Chuetsu earthquake," *Quarterly Report of RTRI*, vol. 48, no. 3, pp. 136–141, 2007.

[10] S. Sharma and W. R. Judd, "Underground opening damage from earthquakes," *Engineering Geology*, vol. 30, no. 3-4, pp. 263–276, 1991.

[11] C. H. Dowding and A. Rozen, "Damage to rock tunnels from earthquake shaking," *ASCE Journal of Geotechnical Engineering*, vol. 104, no. 2, pp. 175–191, 1978.

[12] H. Gercek, "Stability and design of portals in tunnels or galleries," *Kaya Mekanigi Bulteni*, vol. 4, pp. 3–18, 1990.

[13] D. Peila and S. Pelizza, "Criteria for technical and environmental design of tunnel portals," *Tunnelling and Underground Space Technology*, vol. 16, pp. 133–150, 2002.

[14] K. Konagai, "Data archives of seismic fault-induced damage," *Soil Dynamics and Earthquake Engineering*, vol. 25, no. 7–10, pp. 559–570, 2005.

[15] J. Penzien, "Seismically induced racking of tunnel linings," *Earthquake Engineering & Structural Dynamics*, vol. 29, no. 5, pp. 683–691, 2000.

[16] Y. M. A. Hashash, J. J. Hook, B. Schmidt, and J. I-Chiang Yao, "Seismic design and analysis of underground structures," *Tunnelling and Underground Space Technology*, vol. 16, no. 4, pp. 247–293, 2001.

[17] K. Yoshikawa, "Investigation about past earthquake disasters of railway tunnels," *Quarterly Report of RTRI*, vol. 22, no. 3, pp. 103–111, 1981.

[18] W. L. Wang, T. T. Wang, J. J. Su, C. H. Lin, C. R. Seng, and T. H. Huang, "Assessment of damage in mountain tunnels due to the Taiwan Chi-Chi earthquake," *Tunnelling and Underground Space Technology*, vol. 16, no. 3, pp. 133–150, 2001.

[19] S. Kontoe, L. Zdravkovic, D. M. Potts, and C. O. Menkiti, "Case study on seismic tunnel response," *Canadian Geotechnical Journal*, vol. 45, no. 12, pp. 1743–1764, 2008.

[20] T. D. O'Rourke, S. H. Goh, C. O. Menkiti, and R. J. Mair, "Highway tunnel performance during the 1999 Duzce earthquake," in *Proceedings of the 15th International Conference on Soil Mechanics and Foundation Engineering*, vol. 2, Balkema, Rotterdam, Netherlands, pp. 1365–1368, 2001.

[21] T. B. Li, "Failure characteristics and influence factor analysis of mountain tunnels at epicenter zones of great Wenchuan earthquake," *Journal of Engineering Geology*, vol. 16, no. 6, pp. 742–750, 2008.

[22] T. Li, "Damage to mountain tunnels related to the Wenchuan earthquake and some suggestions for aseismic tunnel construction," *Bulletin of Engineering Geology and the Environment*, vol. 71, no. 2, pp. 297–308, 2012.

[23] Z. Wang, B. Gao, Y. Jiang, and S. Yuan, "Investigation and assessment on mountain tunnels and geotechnical damage after the Wenchuan earthquake," *Science in China Series E: Technological Sciences*, vol. 52, no. 2, pp. 546–558, 2009.

[24] J. X. Lai, S. Y. He, J. L. Qiu et al., "Characteristics of seismic disasters and aseismic measures of tunnels in Wenchuan earthquake," *Environmental Earth Sciences*, vol. 76, no. 2, pp. 1–19, 2017.

[25] H. Yu, J. Chen, A. Bobet, and Y. Yuan, "Damage observation and assessment of the Longxi tunnel during the Wenchuan earthquake," *Tunnelling and Underground Space Technology*, vol. 54, pp. 102–116, 2016.

[26] O. Kusakabe, J. Takemura, A. Takahashi, J. Izawa, and S. Shibayama, "Physical modeling of seismic responses of underground structures," in *Proceedings of the The Twelfth International Conference of International Association for Computer Methods and Advances in Geomechanics*, pp. 1459–1474, Goa, India, 2008.

[27] T. Yamada, H. Nagatani, H. Igarashi, and A. Takahashi, "Centrifuge model tests on circular and rectangular tunnels subjected to large earthquake-induced deformation," in *Proceedings of the Third Symposium on Geotechnical Aspects of Underground Construction in Soft Ground*, C. W. W. Ng, H. W. Huang, and G. B. Liu, Eds., CRC Press, London, UK, pp. 673–678, 2002.

[28] Wang M. N., Study on shock absorption technology of underground structure in high earthquake intensity area. Ph.D. dissertation, Southwest Jiaotong University, Chengdu, China, 1999, in Chinese.

[29] Z. Y. Chen and H. Shen, "Dynamic centrifuge tests on isolation mechanism of tunnels subjected to seismic shaking," *Tunnelling and Underground Space Technology*, vol. 42, pp. 67–77, 2014.

[30] L. Li and C. He, "Large-scale shaking table test for shallow-buried unsymmetrical tunnel Chinese," *Journal of Rock Mechanics and Engineering*, vol. 30, no. 12, pp. 2540–2548, 2011, in Chinese.

[31] D. Xu, Y. Chen, and J. Fang, "Analysis of deformation and failure of Longxi tunnel in the duwen highway," *Resources Environment & Engineering*, vol. 23, no. 9, pp. 76–84, 2009, in Chinese.

[32] Y. Yu, *Seismic Damage Mechanism of Secondary Lining of Mountain Tunnel*, Doctoral thesis in Chinese, Institute of Engineering Mechanics, China Earthquake Administration, Harbin, China, 2013.

[33] Y. Chen and D. Xu, *FLAC/FLAC3D Examples of Foundation and Engineering*, China Water & Power Press, Beijing, China, 2009, in Chinese.

[34] H. Ding, F. He, Y. Xie, and X. Xu, *Finite Element Method in Elastic-Plastic Mechanics*, China Machine Press, Beijing, China, 1998, in Chinese.

[35] C. He and A. Koizumi, "Study on seismic behavior and seismic design methods in transeverse direction of shield tunnels," *Structural Engineering and Mechanics*, vol. 11, no. 6, pp. 651–662, 2001.